Supporting Information

Kulić *et al.* 10.1073/pnas.0800031105

SI Text

Perpendicular Microtubule Fluctuations of Kinesin Knocked Down Cells. To determine the origin of the observed microtubule network fluctuations we have knocked down kinesin by treating the cells with dsRNA against kinesin heavy chain.

Templates for *in vitro* transcription were generated by using the primers 5′-AATACGACTCACTATAGGGaGAACATCATCCTCACCAACG-3′ and 5′-TAATACGACTCACTATAGGGgTTCTTATCCTCGTGCACACT-3′ to amplify the 500-bp segment from the N terminus of the kinesin heavy chain (KHC) gene. RNAi treatment was performed as described by Ling *et al.* (1). dsRNA-treated cells remained fully viable as they were able to attach and spread on the substrate.

Analysis Method. To compare the lateral fluctuations in ordinary versus KHC RNAi-treated cells, we selected cell sections with high orientational alignment of microtubules and calculated intensity linescans along the perpendicular direction to the mean microtubule direction (Fig. S2). The movies were background-subtracted before analysis to avoid bias from variable background levels. For each linescan we evaluated the intensity cross-correlation $C(\Delta t)$ between the linescans separated in time as function of the time lag Δt between frames (Fig. S3). The cross-correlation is defined as

$$C(\Delta t) = \left\langle \frac{\int I(t+\Delta t,x)I(t,x)dx}{\sqrt{\int I^2(t+\Delta t,x)dx \int I^2(t,x)dx}} \right\rangle_t,$$

where $I(t,x)$ denotes the intensity in the mCherry (red) channel at the position x (along the linescan) at the time point t and $\langle\ \rangle_t$ denotes the mean over all time lapse frames. The integration is performed over the whole interval of the linescan. A physical interpretation of this observable can be obtained as follows. The intensity profile can be approximated as a superposition of Gaussian intensity profiles of individual microtubules, i.e.,

$$I(t,x) = \sum_{k=1}^{N} A_k e^{-\frac{(x-x_k(t))^2}{\sigma_k}},$$

where A_k and $\sqrt{\sigma_k}$ stand for the intensity amplitude and spread of intensity (variance) and $x_k\ (_t)$ denotes the position of the kth microtubule along the linescan. In our case where all of the amplitudes A_k and σ_k are of the same order, i.e., respectively, $A_k = A$ and $\sigma_k = \sigma$, simple calculation shows that

$$C(\Delta t) = \left\langle \frac{1}{N} \sum_{k=1}^{N} e^{-\Delta x_k^2(\Delta t)/2\sigma} \right\rangle_t,$$

where $\Delta x_k\ (\Delta t)$ is the displacement of the kth microtubule. For short times we have small displacements $\Delta x_k\ (t) \ll 2\sigma$ and the upper expression can be Taylor-expanded:

$$1 - C(\Delta t) \approx \frac{1}{2\sigma N} \sum_{k=1}^{N} \langle \Delta x_k^2(\Delta t) \rangle_t.$$

Therefore, the expression 1-$C(\Delta t)$ has the interpretation of the perpendicular mean square microtubule displacement (averaged over all N microtubules and timeframes of the linescan) divided by the squared optical thickness 2σ of the microtubule fluorescence image. In our case $\sigma \approx (\lambda/2)^2$ coincides with the width of a point spread function at the emission wavelength 595 nm of mCherry.

SI Results

We have compared the perpendicular microtubule fluctuations of sections of WT cells with RNAi kinesin heavy chain (KHC-RNAi)-treated cells (both cell types Cytochalasin D-treated). The measurements were performed in nine independent locations of six different KHC-RNAi cells and in 20 different locations of 10 different WT cells. The KHC-RNAi cells show significantly reduced microtubule fluctuations as compared with the WT cells indicating a strong contribution of kinesin motors in the generation of cytoskeletal noise in these cells.

Analysis of Exponential Velocity Relaxation Events. We have examined the occurrence of nonsteady velocity events (one of which is shown in Fig. 1*a*) in 36 peroxisome traces. In nine traces (25%) we have detected 20 such events that were longer in duration than 150 ms. These segments of peroxisome trajectories were well fitted by an exponential function $x(t) = \Delta L\ [\exp(-t/t_{\rm rel}) - 1]$ with ΔL being the stored length and $t_{\rm rel}$ the relaxation time, with a coefficient of determination ($R_{\rm square}$) larger than 0.95. A compilation of such events together with the corresponding fits is shown in Fig. S4. The statistics of the fitted stored lengths and relaxation times are shown in Fig. S5.

The relaxation times extracted from the observed events (Figs. S4 and S5) are in the range of 40–950 ms. From the wavelength-relaxation time relation for a semiflexible filament $t_{\rm rel} \approx 4L^4\eta/[\pi^3 \ln(L/\pi a)B]$ with ($B \approx 2 \times 10^{-23}$ nm^2 the microtubule bending stiffness, $\eta \approx 10^{-2}$ Pa s the cytoplasmic viscosity, L the length of the buckled segment, and $a = 25$ nm the microtubule diameter) we obtain a rough estimate of the microtubule segment lengths involved in these relaxations: $L \approx 7$–$15\ \mu$m. The estimated segment lengths L are significantly larger than the estimated stored lengths ΔL (0.2–1.3 μm) indicating that that microtubules are indeed only weakly deformed during the process. Taking into account that single motors can generate forces $F \approx 1$–5 pN, capable of buckling microtubules and injecting stored length over scales $L \approx \sqrt{B/F}$ (a few micrometers), we conclude that the observed timescales and stored lengths are consistent with the interpretation of motor-induced microtubule buckling followed by rapid elastic unbuckling events. Note that the initial relaxation velocities during such unbuckling events can be very high: $v_{\rm max} \approx \Delta L/t_{\rm rel}$ (up to $\approx$10 s of μm/s), well in excess of cytoplasmic motor speeds ($\approx$1 μm/s).

In some cases (three of nine trajectories) two or more relaxation events could be observed within the same peroxisome trace (see the last row of four plots in Fig. S4). Remarkably, such events (when occurring within the same trace) not only showed similar relaxation times and stored lengths but in at least one case very striking correlations (in the fine structure superimposed onto the exponentially relaxing position vs. time; see Fig. S6). This indicates that a reproducible repetitive process might be causing several such relaxation events separated in time by $\approx$4 s and space $\approx$4.5 μm. The detailed origin of such repetitive events will be the focus of our future studies.

Behavior Expected for Random Kinesin–Dynein Switching on Immobile Microtubules. Here we extend the discussion in the main text of the expected behavior for a cargo that randomly switches directions, for example because it carries kinesin and dynein on immobile microtubules (see Fig. S7).

We assume that there is no net aggregation of cargos on either microtubule end (as is the case for our S2 cells). In this case the processive times t^+ and t^- and mean velocities v^+ and v^- (in plus and minus direction, respectively) have to satisfy the zero net velocity condition: $v^+t^+/t^* = v^-t^-/t^*$ with $t^* = t^- + t^+$. In addition we assume that switching and running behavior of motors has no history dependence. As known from probability theory under such conditions (lack of bias and history independence) on long timescales $t \gg t^*$ the cargo motion becomes diffusive. Depending on the size of the observation time window T_{obs} one would expect to observe two different behaviors of the mean square displacement vs. lag time. If $T_{obs} < t^*$ (motors switch on longer times than observation interval), then motors of either polarity move the cargo in plus or minus direction at constant velocities and the mean square displacement (MSD) vs. time lag consists of a single line with slope 2 (ballistic motion) on the log-log scale. If the observation time is long enough and the motors switch fast enough, $T_{obs} > t^*$, one would expect to observe a crossover from slope 2 to 1, ballistic to diffusive behavior at time lags $\approx t^*$.

This expected behavior has to be contrasted to the experimentally observed MSD vs. time lag (Fig. 1 *c*). The complete absence of the ballistic regime from the majority of trajectories and the occurrence of a stable 3/2 scaling exponent (over approximately two decades) indicates that the presented naïve random kinesin–dynein switching model is not an appropriate description of peroxisome motion in *Drosophila* S2 cells.

Mean Square Displacement Exponents at Long Timescales. We have analyzed the mean square displacement (MSD) exponent of 55 peroxisomes from 11 different cells over the time interval from 1 to 60 s. A subset of the population consisting of ≈20% peroxisomes (10 peroxisomes) displayed a confined motion with their MSD saturating at timescales ≈6–14 s. The remaining peroxisome population ($n = 45$) moved in an unbound manner. The MSD(Δt) was calculated for each peroxisome in this second population and fitted on the interval $\Delta t = 2$–16 s to a power-law $\mathrm{MSD}(\Delta t) = c\,\Delta t^{\gamma}$. The exponents γ are broadly scattered around the mean value 1.05 (standard deviation 0.30) (see Fig. S1).

1. Ling SC, Fahrner PS, Greenough WT, Gelfand VI (2004) Transport of *Drosophila* fragile X mental retardation protein-containing ribonucleoprotein granules by kinesin-1 and cytoplasmic dynein. *Proc Natl Acad Sci USA* 101:17428–17433.

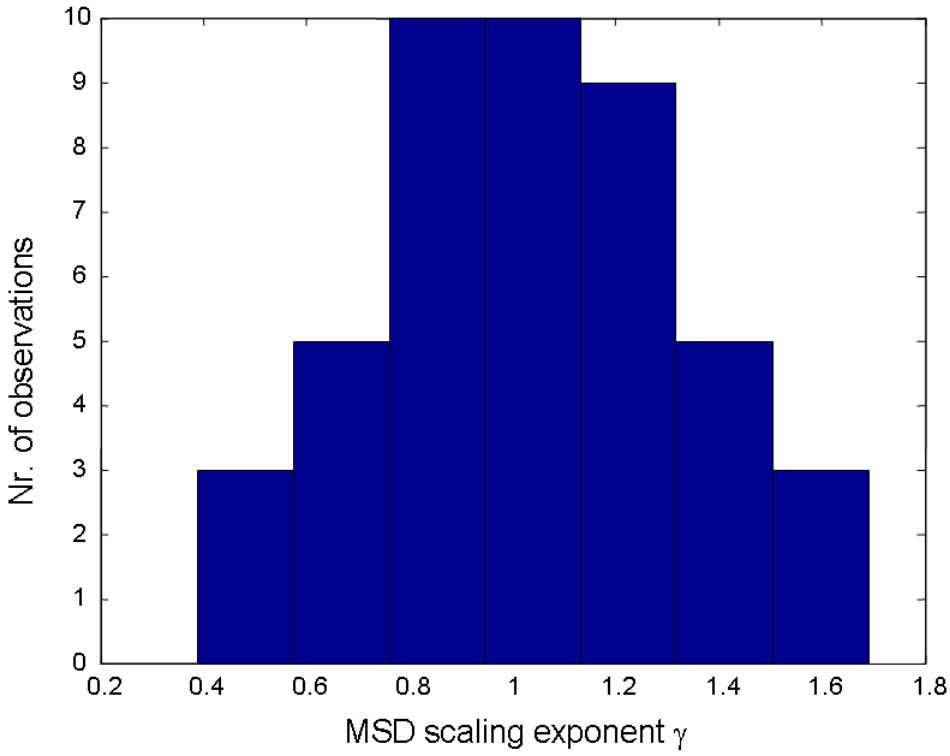

Fig. S1. The MSD scaling exponent distribution for $n = 45$ peroxisomes at time scales 2–16 s.

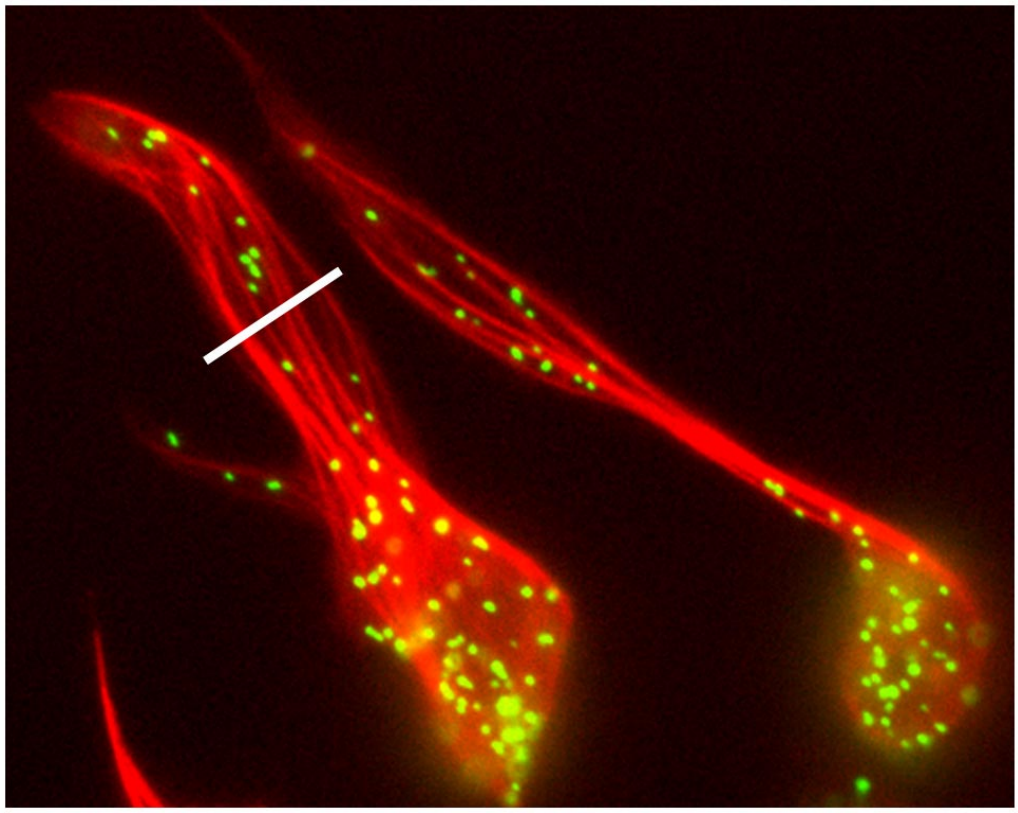

Fig. S2. The linescan correlation method for quantifying lateral microtubule fluctuations (Movie S13).

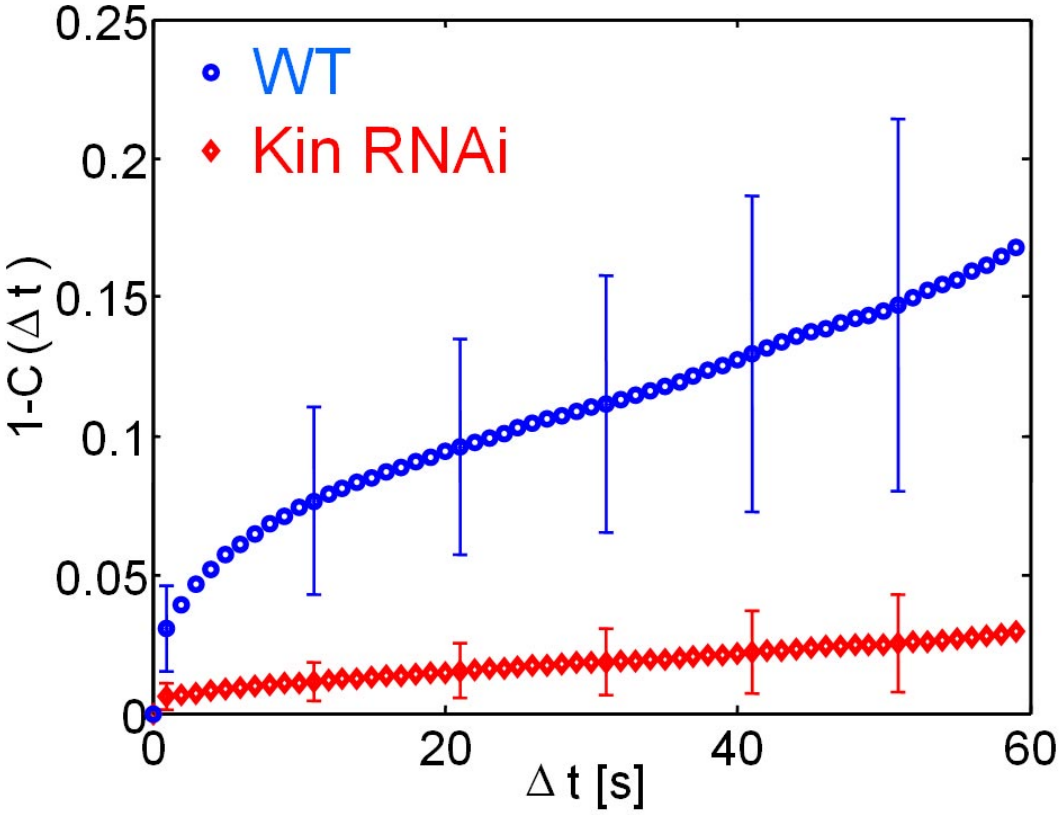

Fig. S3. The loss of intensity–intensity correlation as function of the time lag Δt between time-lapse image frames.

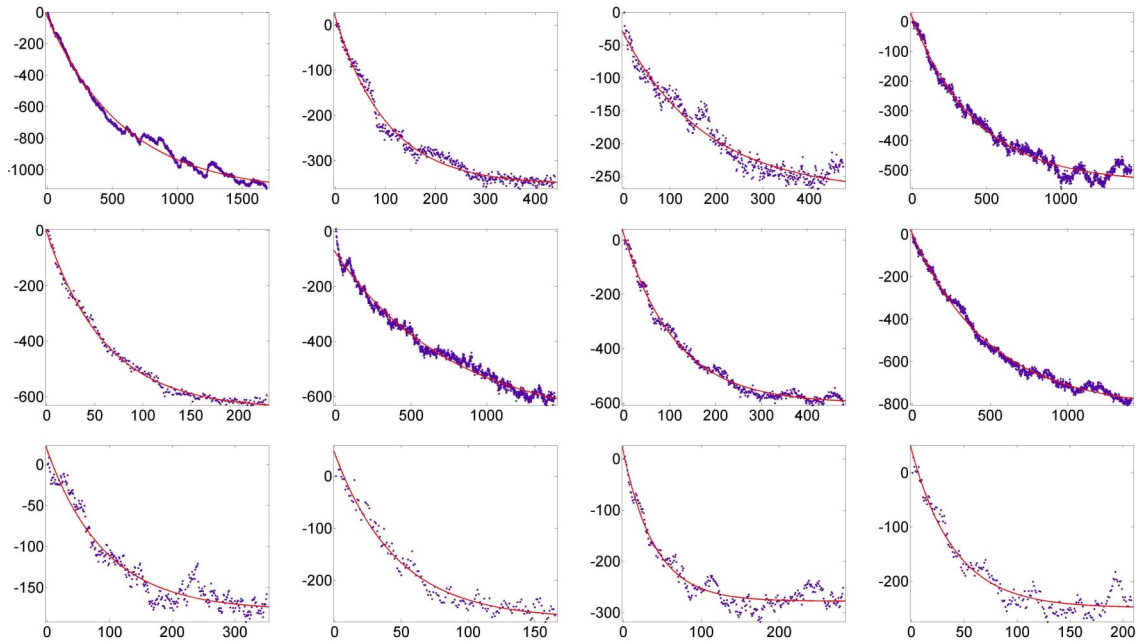

Fig. S4. Examples of velocity relaxations occurring over various time and length scales. *x* axis, time in milliseconds; *y* axis, released length in nanometers. The red lines are best exponential fits. The four plots in the last row all came from a single peroxisome trajectory, which showed four relaxation events. In each graph time has been shifted to the start of the event shown.

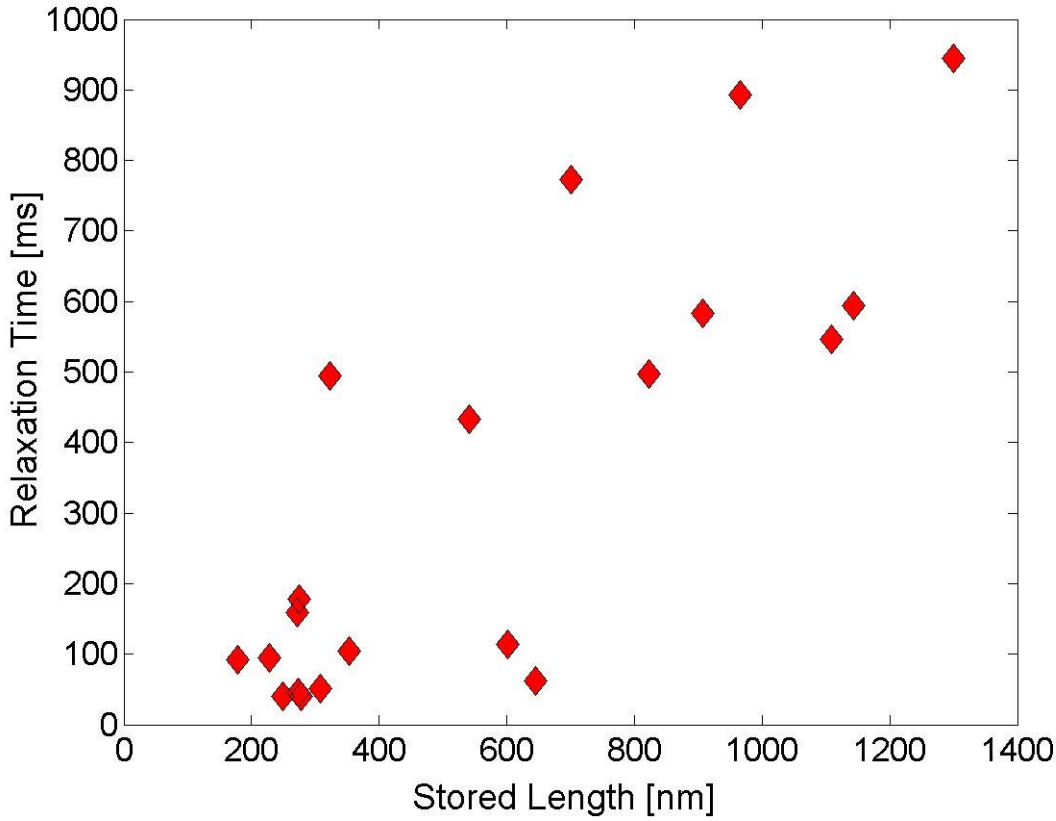

Fig. S5. The fitted relaxation times vs. relaxation lengths of 20 different relaxation events from nine different peroxisomes' trajectories.

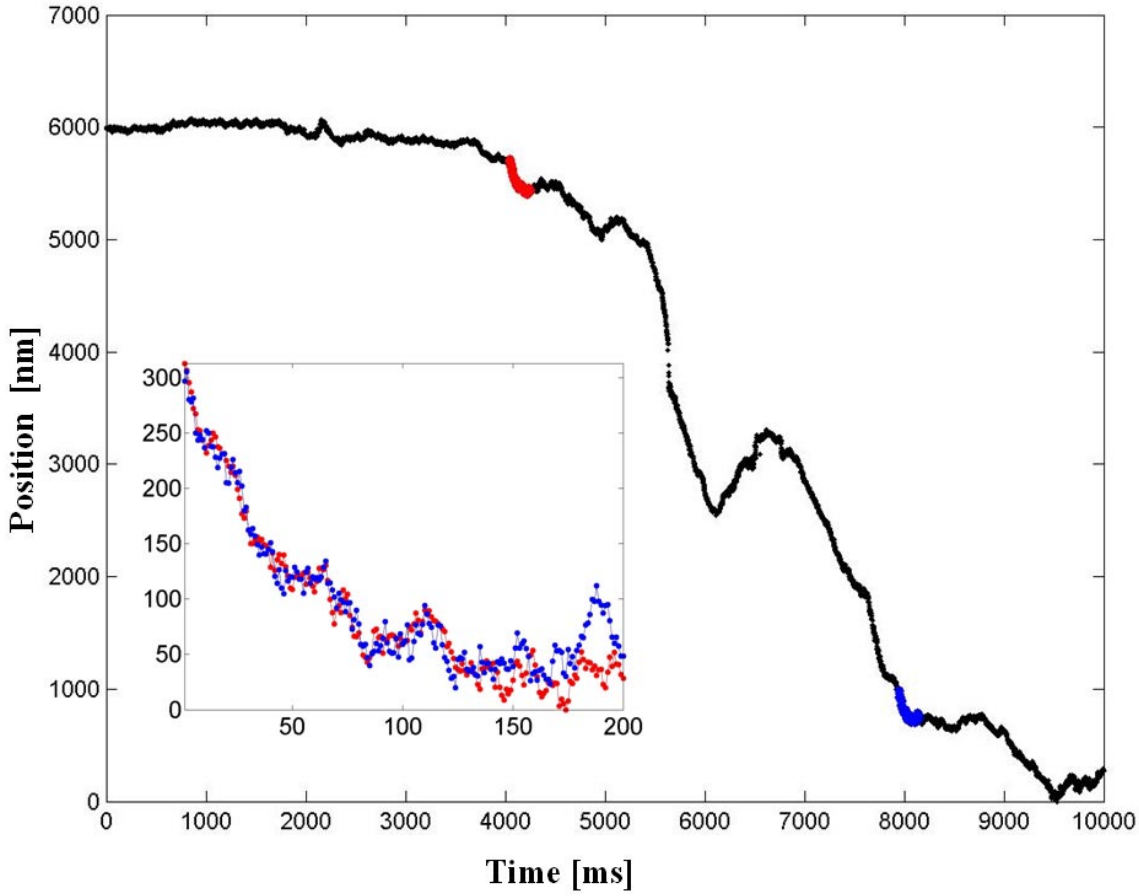

Fig. S6. Example of a peroxisome trace (black dots) exhibiting multiple relaxation events. Two such events (highlighted in blue and red) lasting >150 ms show a high correlation (0.96, see *Inset*), indicating the possibility of a repetitive mechanism behind these relaxations.

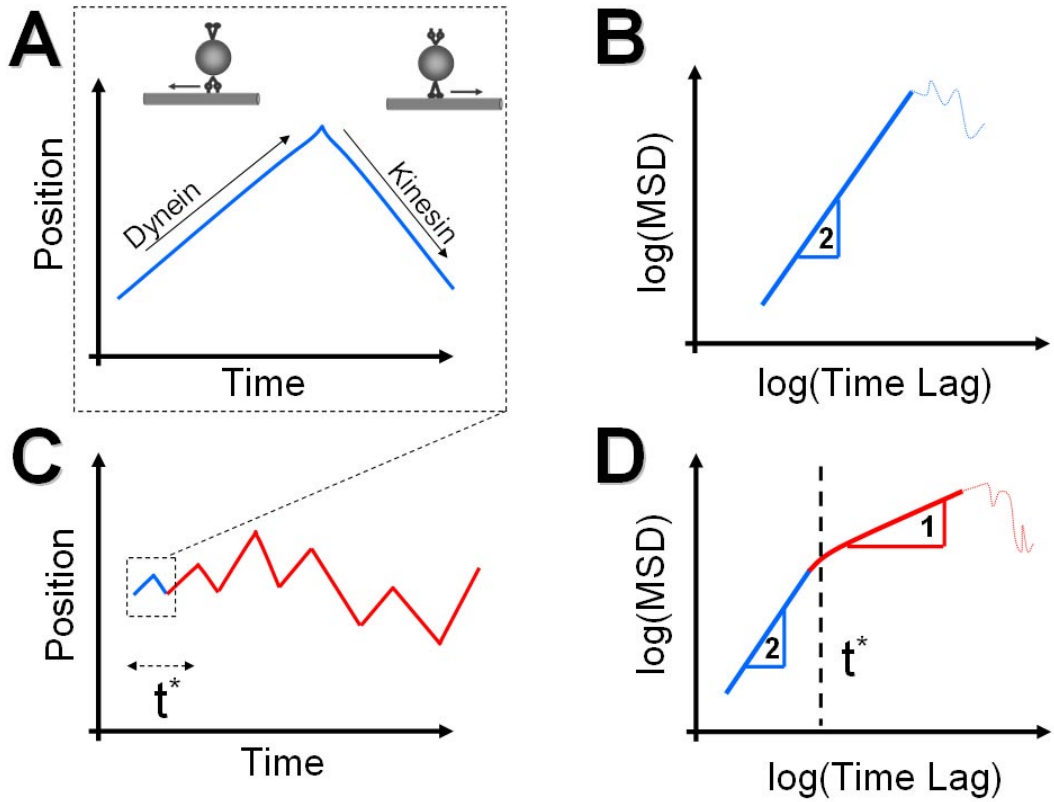

Fig. S7. Schematic outline of scaling behavior expected from random motor switching. A, if the observation time interval is shorter or comparable to the typical motor switching time t^* we expect: *B*, a single power-law scaling of the MSD vs. lag time with slope 2 (thick line in B) followed by a region with insufficient statistics (thin dotted line). C, if motor switching occurs fast compared to the observation interval, *D*, the MSD scaling shows two exponents, 2 at short times (ballistic) followed by exponent 1 (diffusive) at times lags longer than t^*.

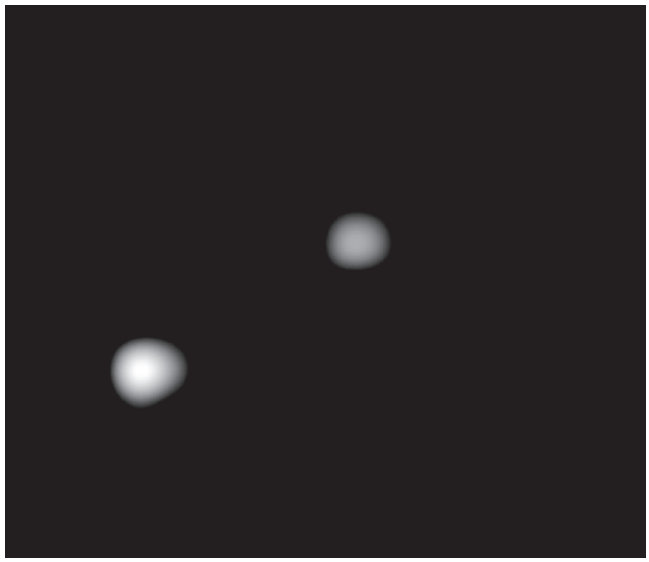

Movie S1. TIRF movie sequence of two EGFP-labeled peroxisomes moving in unison over 20 s (corresponds to Fig. 1*b*). Every 10th frame of the original movie has been selected (10,000 frames acquired at 500 frames per second) and played back at 100 frames per second.

Movie S1

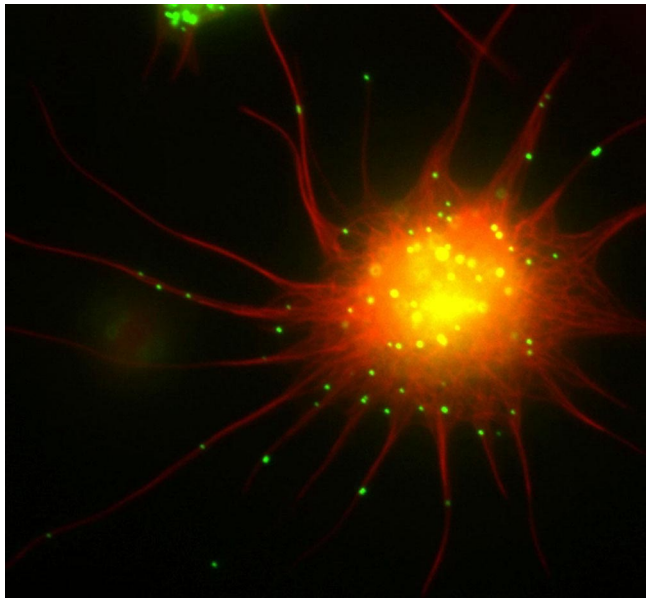

Movie S2. Two-color fluorescence time lapse sequence of a Cytochalasin D-treated S2 cell with microtubules shown in red and peroxisomes in green. The movie was acquired at one frame per second and is played back at eight frames per second.

Movie S2

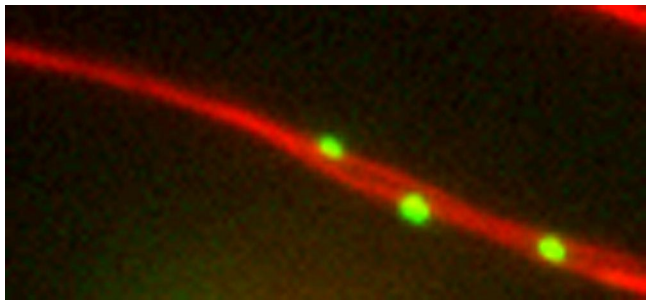

Movie S3. Movie sequence corresponding to Fig. 2*a*. A microtubule from Movie S2 is seen buckling out of a bundle in close proximity to a peroxisome. The movie was acquired at one frame per second and is played back at eight frames per second. See also Fig. 2*a*.

Movie S3

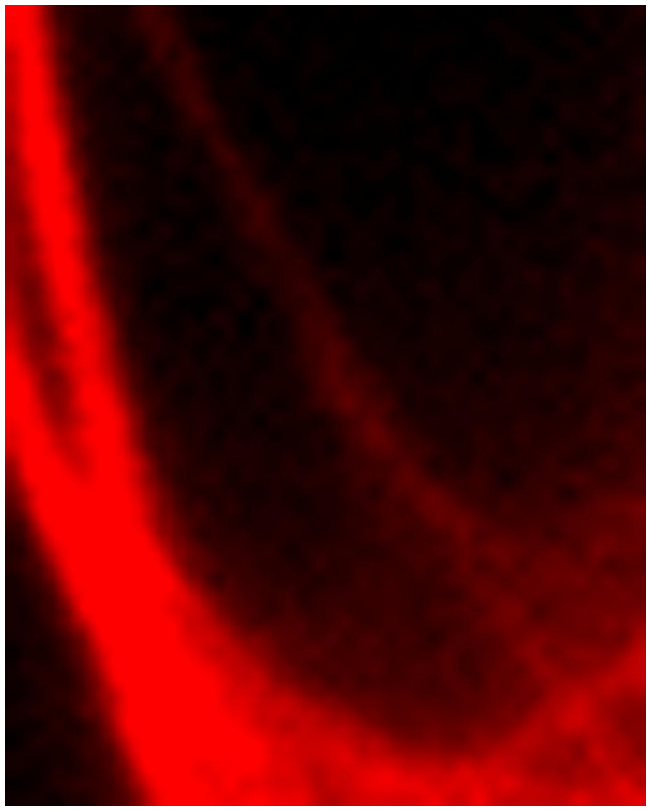

Movie S4. Movie sequence corresponding to Fig. 2*b*. A microtubule from Movie S2 slides along the process and strongly buckles, close to the end of the sequence. The movie was acquired at one frame per second and is played back at eight frames per second.

Movie S4

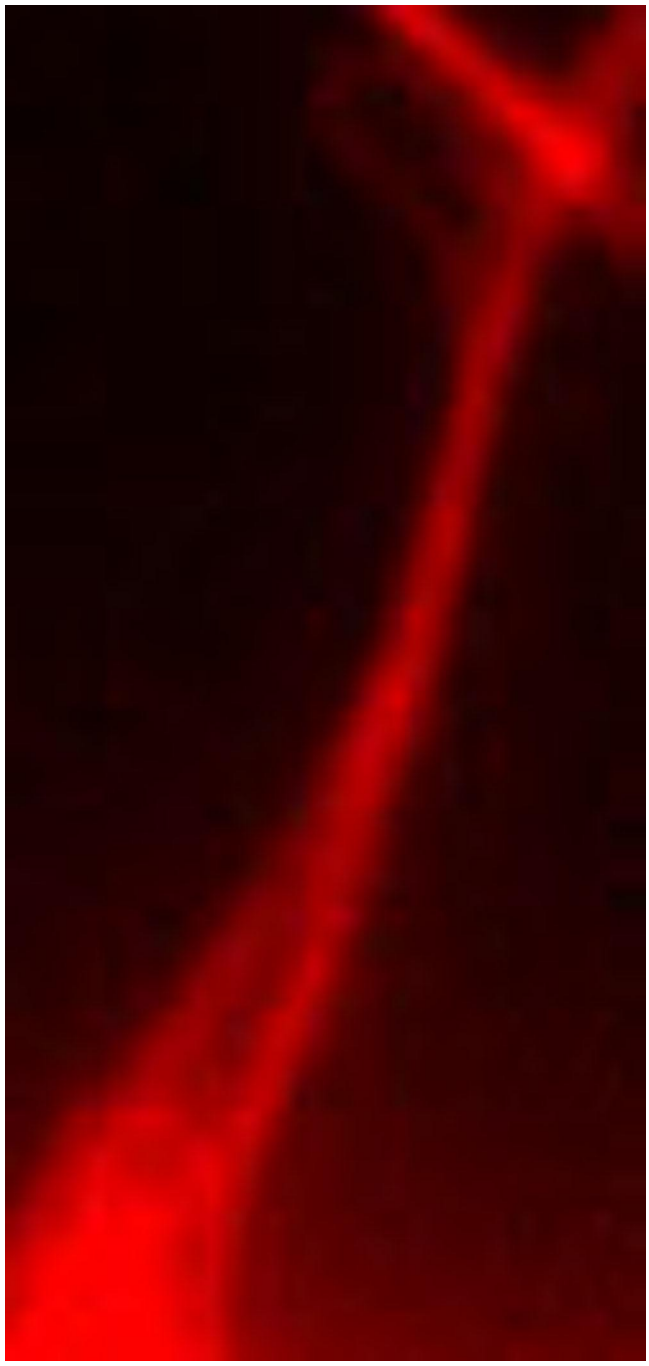

Movie S5. Movie sequence corresponding to Fig. 2*c*. A microtubule loop from Movie S2 forms and is transported down the length of a process at 0.8 μm/s. The movie was acquired at one frame per second and is played back at eight frames per second.

Movie S5

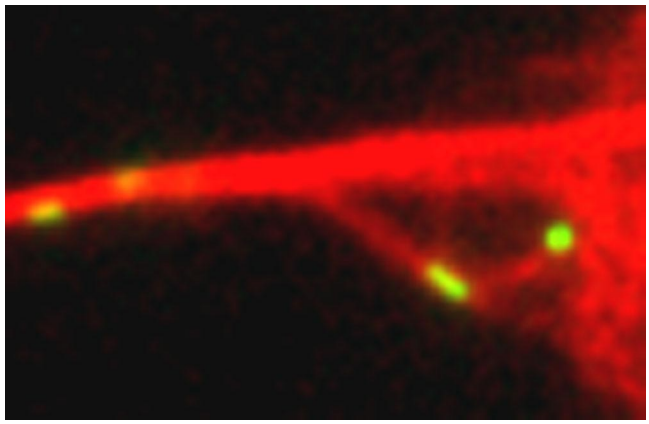

Movie S6. Movie sequence corresponding to Fig. 3*a*. A peroxisome dynamically clamps two microtubules as it moves along both, releases one of them, and continues to the right (passing another immobile peroxisome) while the microtubules splay apart. The movie was acquired at one frame per second and is played back at eight frames per second.

Movie S6

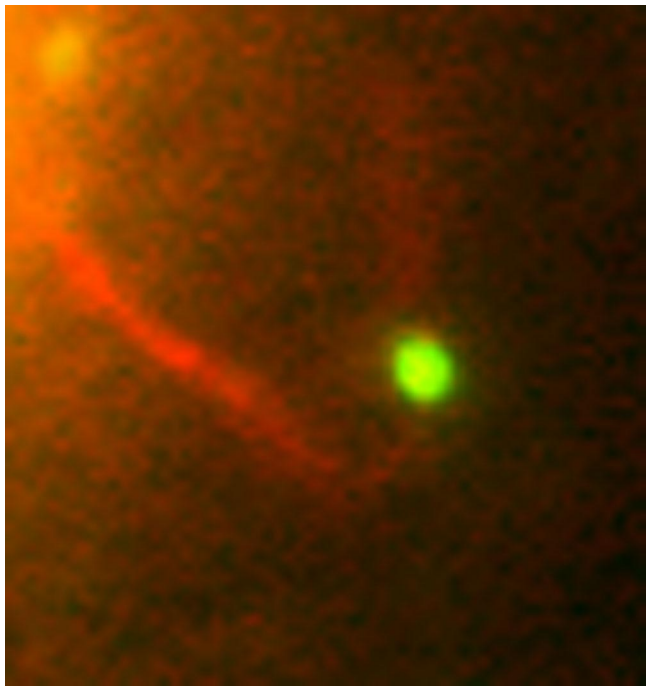

Movie S7. Movie sequence corresponding to Fig. 3*b*. A peroxisome coincides with a strongly dynamically rearranging microtubule bundle kink. The bundle splits into several microtubules, which converge at the vesicle position. The movie was acquired at 30 frames per second, averaged over five subsequent frames (frame rate six frames per second), and is played back at eight frames per second.

Movie S7

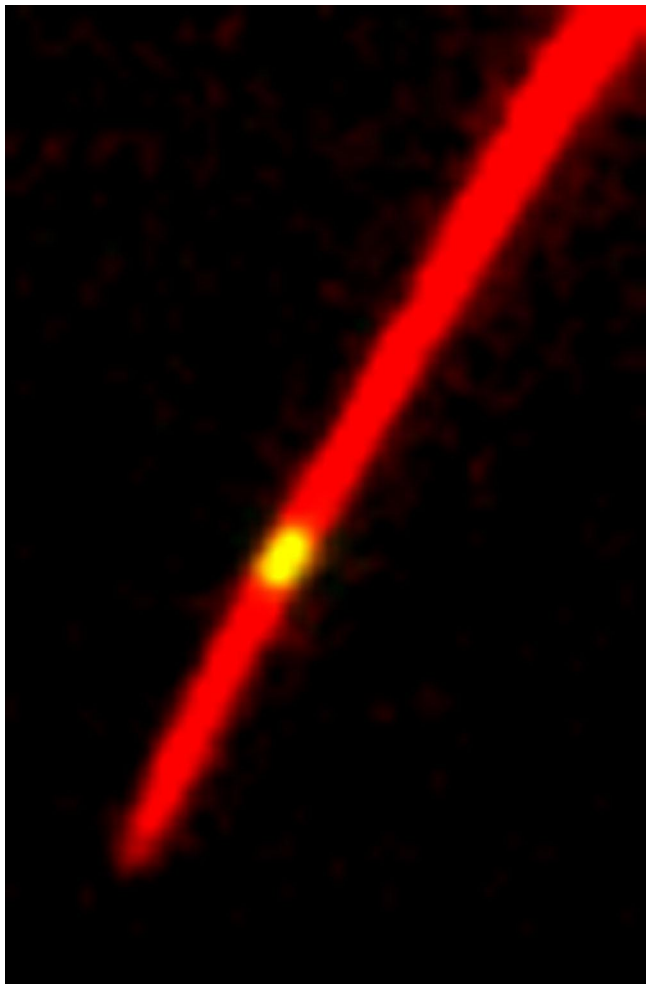

Movie S8. Movie sequence corresponding to Fig. 3*c*. A microtubule tip and the peroxisome move together. The movie was acquired at one frame per second and is played back at eight frames per second.

Movie S8

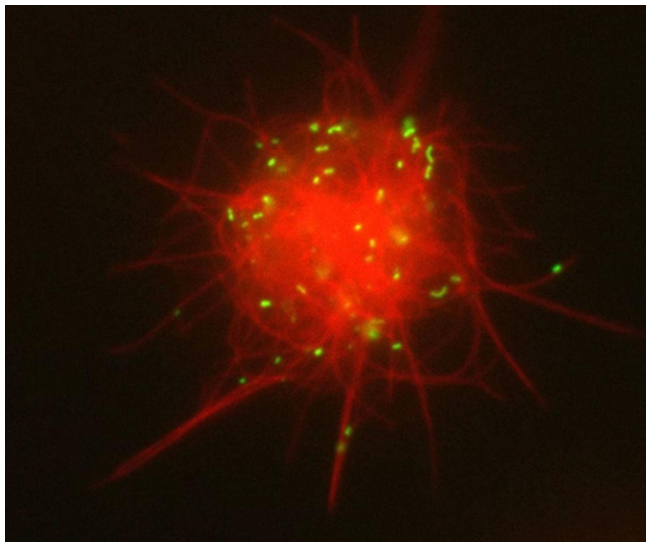

Movie S9. Movie sequence corresponding to Fig. 4. Two-color fluorescence time lapse sequence of a Cytochalasin D-treated S2 cell with microtubules shown in red and peroxisomes in green. The movie was acquired at one frame per second and is played back at eight frames per second.

Movie S9

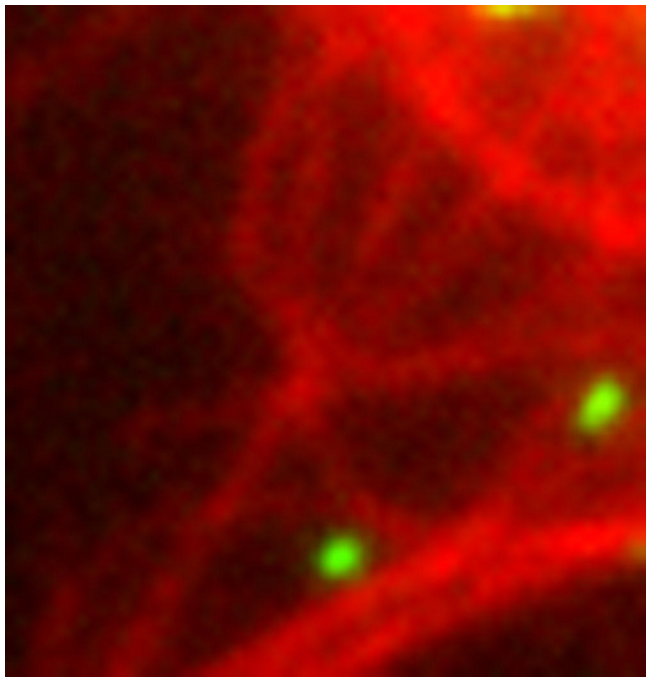

Movie S10. Movie sequence corresponding to Fig. 4*a*. A dynamic microtubule cross-linking point ("hub") from Movie S9. The movie was acquired at one frame per second and is played back at eight frames per second.

Movie S10

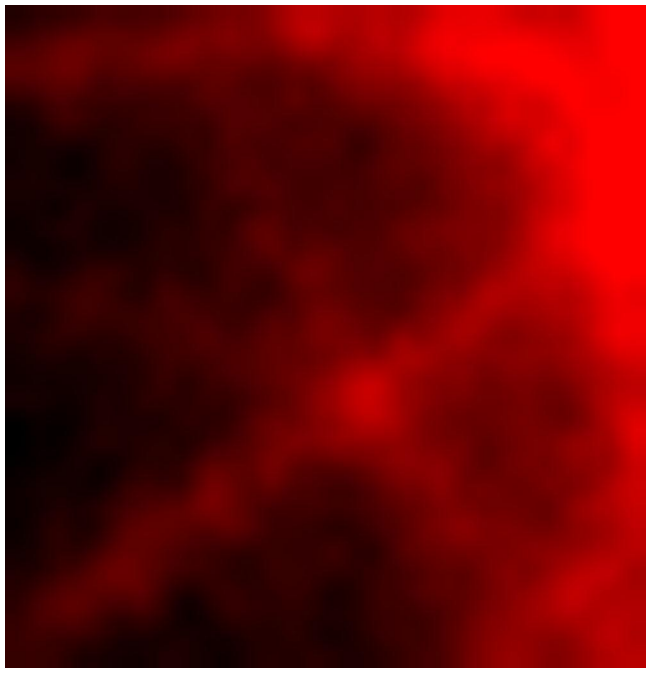

Movie S11. Movie sequence corresponding to Fig. 4*b*. Another dynamic microtubule cross-linking point ("hub") from Movie S9. The movie was acquired at one frame per second and is played back at eight frames per second.

Movie S11

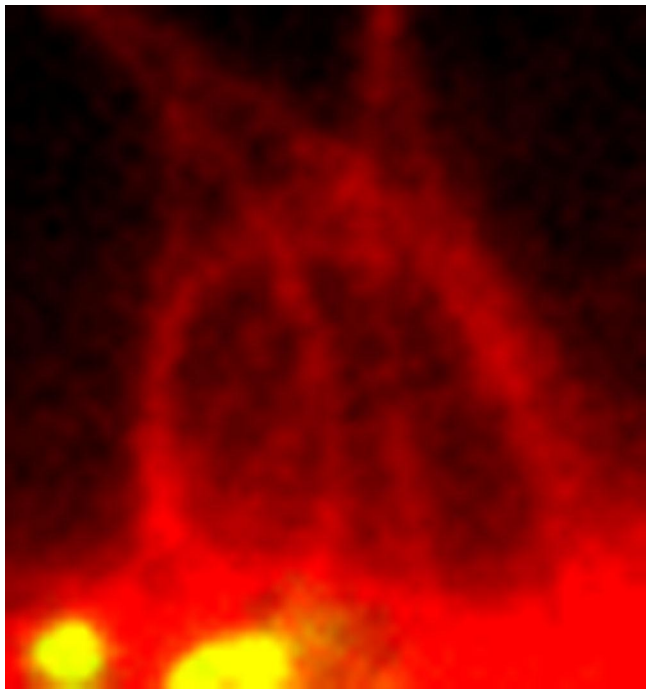

Movie S12. Movie sequence corresponding to Fig. 4*c*. Another microtubule cross-linking point ("hub") from Movie S9. The movie was acquired at one frame per second and is played back at eight frames per second.

Movie S12

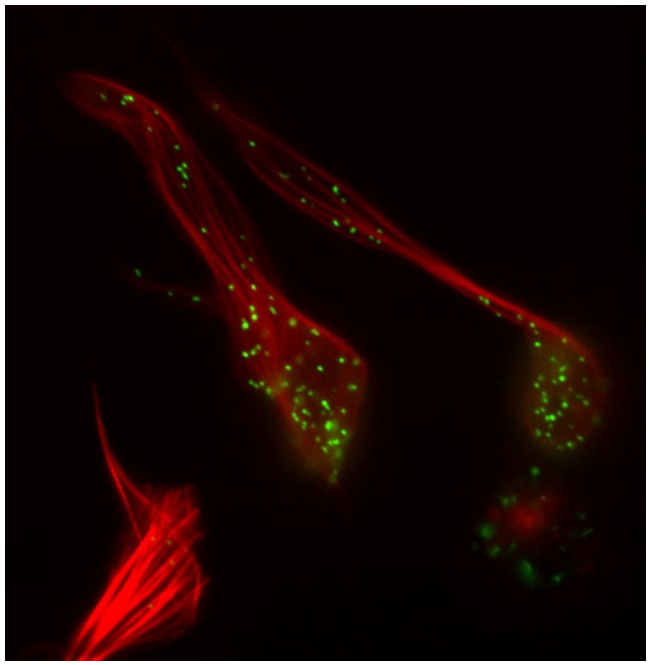

Movie S13. RNAi kinesin heavy chain knocked down cells shown dramatically reduced microtubule motion. The movie was acquired at one frame per second and is played back at eight frames per second.

Movie S13